Progress In Electromagnetics Research, PIER 64, 1–21, 2006

NUMERICAL ANALYSIS OF OPTICAL WAVEGUIDES BASED ON PERIODIC FOURIER TRANSFORM

K. Watanabe

Department of Information and Communication Engineering
Faculty of Information Engineering
Fukuoka Institute of Technology
3-30-1 Wajirohigashi, Higashi-ku, Fukuoka 811-0295, Japan

K. Kuto

Department of Intelligent Mechanical Engineering
Faculty of Engineering
Fukuoka Institute of Technology
3-30-1 Wajirohigashi, Higashi-ku, Fukuoka 811-0295, Japan

Abstract—Periodic Fourier transform is formally introduced to analyses of the electromagnetic wave propagation in optical waveguides. The transform make the field components periodic and they are then expanded in Fourier series without introducing an approximation of artificial periodic boundary. The proposed formulation is applied to two-dimensional slab waveguide structures, and the numerical results evaluate the validity and show some properties of convergence.

1. INTRODUCTION

Series of waveguide transitions where the cross section of a waveguide structure changes in the direction of optical propagation are widely used in the design of integrated optical circuits, for example, junctions, tapers, and branches. Many numerical approaches such as the coupled-mode theory (CMT) [1, 2], the beam-propagation method (BPM) [3, 4], and the Fourier series expansion method (FSEM) [5–9] have been developed to analyze in optical waveguides. The standard CMT is based on the overlap integrals of eigenmode fields and requires solving the dispersion equation for each waveguide section to obtain the eigenmode fields. However, choosing adequate initial values to solve the dispersion equation is not always easy and, also, the overlap

integrals are time-consuming in various problems. The standard BPM provides a unified treatment of various guided wave structures within the para-axial approximation. The advantage of the method is that it uses a simple numerical algorithm and can be easily applied to various kinds of waveguide transitions but the reflected wave fields are inherently ignored in the analysis because of the para-axial approximation introduced in the direction of optical propagation. FSEM introduce an artificial periodicity in the transverse direction and the electromagnetic fields are expanded in the Fourier series. Then wave propagation inside each straight waveguide section is solved by an eigenvalue analysis and the connections at the waveguide transitions are realized by equating the Fourier coefficients corresponding to the tangential components of E and H fields. To reduce the truncation number for the Fourier series expansions, the artificial period must be kept small because larger period makes the convergence slower. However, the artificial period has to be large when applied to a series of waveguide transitions in which the radiation occurs with a wide propagation angle. To avoid the difficulty, several approaches have been proposed in which absorbing layer is introduced to absorb the radiation [8, 9], though the propagation constants of guided modes in each straight waveguide section become complex even when using lossless materials.

This paper proposes a novel numerical approach for waveguide transition problems with the use of the periodic Fourier transform developed by Nakayama [10, 11]. The periodic Fourier transform was proposed to analyze the scattering problems of periodic surfaces with finite extent. Let $f(x)$ be a function satisfying conditions (f1)–(f3) shown in Appendix. Then the periodic Fourier transform is defined by

$$\widetilde{f}(x;\alpha) \equiv \sum_{m=-\infty}^{\infty} f(x - m\,d)\, e^{-i\,\alpha(x-m\,d)} \tag{1}$$

and the inverse transform is given by

$$f(x) = \frac{d}{2\,\pi} \int_0^{2\pi/d} \widetilde{f}(x;\alpha)\, e^{i\,\alpha\,x}\, d\alpha. \tag{2}$$

The transform $\widetilde{f}(x;\alpha)$ has a periodic property: $\widetilde{f}(x-d;\alpha) = \widetilde{f}(x;\alpha)$ with the fictitious period d. The conditions (f1)–(f3) ensure the pointwise convergence of Eq. (1) but the transform seems to be practically useful for wider class of functions [10, 11]. In this paper, the periodic Fourier transform is formally applied to the waveguide transition problems, even though the electromagnetic fields

under consideration do not satisfy the conditions (f1)–(f3) and no mathematical proofs of the existence are available at present. The transformed electromagnetic fields become periodic and, then, all field components can be expanded in the Fourier series without introducing the artificial periodic boundary and the absorbing layer. We introduce a discretization in terms of α and then the wave propagation in each waveguide section can be solved as an eigenvalue analysis. Also, the boundary conditions at the waveguide transitions are easily given by equating the respective Fourier coefficients in both sides of the transitions. This scheme is applied to the analysis of structures composed of dielectric slab waveguide transitions and numerical examples validate the effectiveness of the proposed method.

2. FORMULATION

2.1. Setting of the Problem

The series of waveguide transitions under consideration is schematically shown in Fig. 1. The dielectrics are linear and isotropic media, and the permeability of free space is assumed. The geometry is uniform in the y-direction and, also, there is no variation of the field distribution in the y-direction. We consider time-harmonic fields, assuming a time dependence in $\exp(-i\,\omega\,t)$, and the fields are therefore represented by complex vectors depending only on the space variables x and z. The transitions are located at $z = z_\nu$ $(\nu = 0, \ldots, M)$ and the waveguide sections within $z_{\nu-1} < z < z_\nu$ are specified by ν $(\nu = 0, \ldots, M+1)$.

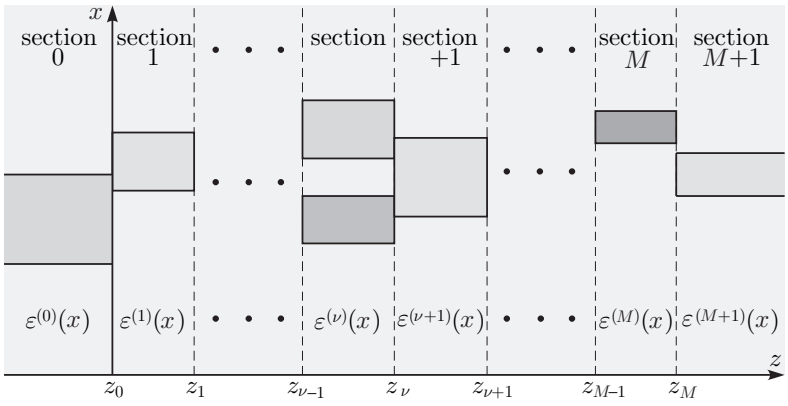

Figure 1. Series of waveguide transitions under consideration.

Each waveguide section is uniform in the z-direction and surrounded by a cladding medium with the relative permittivity ε_s. The relative permittivity distribution in the νth-section is decomposed into the constant part and the nonconstant part and expressed as

$$\varepsilon^{(\nu)}(x) = \varepsilon_s + \varepsilon_c^{(\nu)}(x). \tag{3}$$

The reciprocal of relative permittivity distribution is denoted by $\eta^{(\nu)}(x) = 1/\varepsilon^{(\nu)}(x)$ and decomposed also as

$$\eta^{(\nu)}(x) = \eta_s + \eta_c^{(\nu)}(x). \tag{4}$$

The first term η_s is equal to $1/\varepsilon_s$, but note that the second term $\eta_c^{(\nu)}(x)$ is usually different from $1/\varepsilon_c^{(\nu)}(x)$ because $\varepsilon_c^{(\nu)}(x)$ is zero in the cladding region. For simple expressions, we normalize the fields, namely, the E field by $\sqrt[4]{\mu_0/\varepsilon_0}$, the H field by $\sqrt[4]{\varepsilon_0/\mu_0}$, and the D field by $\varepsilon_0 \sqrt[4]{\mu_0/\varepsilon_0}$, where ε_0 and μ_0 denote the permittivity and the permeability in free space, respectively. In this paper, TE and TM are used to express two fundamental polarizations of the fields. In the TE and the TM polarizations, the E and the H fields are respectively parallel to the y-axis.

2.2. Wave Propagation in Each Waveguide Section

First, we consider the TE polarized wave propagation in each straight waveguide section. From normalized Maxwell's curl equations, we have the following relations:

$$\frac{\partial}{\partial z} H_x(x,z) - \frac{\partial}{\partial x} H_z(x,z) = -i\, k_0\, D_y(x,z) \tag{5}$$

$$\frac{\partial}{\partial z} E_y(x,z) = -i\, k_0\, H_x(x,z) \tag{6}$$

$$\frac{\partial}{\partial x} E_y(x,z) = i\, k_0\, H_z(x,z) \tag{7}$$

where k_0 denotes the wave number in free space. The permittivity distribution is uniform in the z-direction in each waveguide section and the required constitutive relation in the νth-section is written as

$$D_y(x,z) = \varepsilon^{(\nu)}(x)\, E_y(x,z). \tag{8}$$

Introducing the periodic Fourier transform defined by Eq. (1), Eqs. (5)–(8) are transformed into the following relations:

$$\frac{\partial}{\partial z}\widetilde{H}_x(x;\alpha,z) - \left(\frac{\partial}{\partial x} + i\,\alpha\right)\widetilde{H}_z(x;\alpha,z) = -i\,k_0\,\widetilde{D}_y(x;\alpha,z) \tag{9}$$

$$\frac{\partial}{\partial z}\widetilde{E}_y(x;\alpha,z) = -i\,k_0\,\widetilde{H}_x(x;\alpha,z) \tag{10}$$

$$\left(\frac{\partial}{\partial x} + i\,\alpha\right)\widetilde{E}_y(x;\alpha,z) = i\,k_0\,\widetilde{H}_z(x;\alpha,z) \tag{11}$$

$$\widetilde{D}_y(x;\alpha,z) = \varepsilon_s\,\widetilde{E}_y(x;\alpha,z) + \frac{d}{2\,\pi}\int_0^{2\pi/d}\widetilde{\varepsilon}_c^{(\nu)}(x;\alpha-\xi)\,\widetilde{E}_y(x;\xi,z)\,d\xi \tag{12}$$

where Eq. (3) is also used to derive Eq. (12). Since the transforms of all the components of the electromagnetic fields are periodic in terms of x, they can be approximately expanded in the truncated Fourier series. For example, the y-component of the E-field can be written as

$$\widetilde{E}_y(x;\alpha,z) = \sum_{n=-N}^{N}\widetilde{E}_{y,n}(\alpha,z)\,e^{i\,n\,\frac{2\,\pi}{d}\,x} \tag{13}$$

where N denotes the truncation order and $\widetilde{E}_{y,n}(\alpha,z)$ are the nth-order Fourier coefficients. To treat the coefficients systematically, we introduce $(2\,N+1)\times 1$ column matrices; for example, the coefficients of $\widetilde{E}_y(x;\alpha,z)$ are expressed by a column matrix $\widetilde{\boldsymbol{e}}_y(\alpha,z)$ that is defined by

$$\widetilde{\boldsymbol{e}}_y(\alpha,z) = \left(\widetilde{E}_{y,-N}(\alpha,z) \quad \cdots \quad \widetilde{E}_{y,N}(\alpha,z)\right)^t \tag{14}$$

where the superscript t denotes the transpose matrix. Then Eqs. (9)–(12) yield the following relations:

$$\frac{\partial}{\partial z}\widetilde{\boldsymbol{h}}_x(\alpha,z) - i\,k_0\,\boldsymbol{X}(\alpha)\widetilde{\boldsymbol{h}}_z(\alpha,z) = -i\,k_0\,\widetilde{\boldsymbol{d}}_y(\alpha,z) \tag{15}$$

$$\frac{\partial}{\partial z}\widetilde{\boldsymbol{e}}_y(\alpha,z) = -i\,k_0\,\widetilde{\boldsymbol{h}}_x(\alpha,z) \tag{16}$$

$$\boldsymbol{X}(\alpha)\,\widetilde{\boldsymbol{e}}_y(\alpha,z) = \widetilde{\boldsymbol{h}}_z(\alpha,z) \tag{17}$$

$$\widetilde{\boldsymbol{d}}_y(\alpha,z) = \varepsilon_s\,\widetilde{\boldsymbol{e}}_y(\alpha,z) + \frac{d}{2\,\pi}\int_0^{2\pi/d}[\![\widetilde{\varepsilon}_c^{(\nu)}]\!](\alpha-\xi)\,\widetilde{\boldsymbol{e}}_y(\xi,z)\,d\xi. \tag{18}$$

The (n,m)-entries of the matrices $\boldsymbol{X}(\alpha)$ and $[\![\widetilde{\varepsilon}_c^{(\nu)}]\!](\alpha)$ are given by

$$(\boldsymbol{X}(\alpha))_{n,m} = \delta_{n,m}\left(\frac{\alpha}{k_0} + n\,\frac{\lambda_0}{d}\right) \tag{19}$$

$$\left([\![\widetilde{\varepsilon}_c^{(\nu)}]\!](\alpha)\right)_{n,m} = \widetilde{\varepsilon}_{c,n-m}^{(\nu)}(\alpha) \tag{20}$$

where $\delta_{n,m}$ is the Kronecker delta and λ_0 is the wave length in free space. Here, $\widetilde{\varepsilon}_{c,n}^{(\nu)}(\alpha)$ denotes nth-order Fourier coefficients of $\widetilde{\varepsilon}_c^{(\nu)}(x;\alpha)$ and it is given by

$$\begin{aligned}\widetilde{\varepsilon}_{c,n}^{(\nu)}(\alpha) &= \frac{1}{d}\int_0^d \widetilde{\varepsilon}_c^{(\nu)}(x;\alpha)\,e^{-i\,n\,\frac{2\,\pi}{d}\,x}\,dx \\ &= \frac{1}{d}\int_{-\infty}^{\infty} \varepsilon_c^{(\nu)}(x)\,e^{-i\left(\alpha+n\,\frac{2\,\pi}{d}\right)x}\,dx.\end{aligned} \tag{21}$$

Equations (15)–(18) must be satisfied for arbitrary $\alpha \in [0, 2\,\pi/d]$. Here we take $L+1$ sample points $\alpha_l = l\,\Delta\alpha$ $(l = 0,\ldots,L)$ with $\Delta\alpha = (2\,\pi)/(L\,d)$, and apply the trapezoidal rule to approximate the convolution integration. Then Eq. (18) is approximated as

$$\begin{aligned}\widetilde{\boldsymbol{d}}_y(\alpha_l, z) &= \varepsilon_s\,\widetilde{\boldsymbol{e}}_y(\alpha_l, z) \\ &\quad + \frac{1}{2\,L}\left([\![\widetilde{\varepsilon}_c^{(\nu)}]\!](\alpha_l)\,\widetilde{\boldsymbol{e}}_y(\alpha_0, z) + 2\sum_{m=1}^{L-1}[\![\widetilde{\varepsilon}_c^{(\nu)}]\!](\alpha_{l-m})\,\widetilde{\boldsymbol{e}}_y(\alpha_m, z)\right. \\ &\qquad\qquad \left. + [\![\widetilde{\varepsilon}_c^{(\nu)}]\!](\alpha_{l-L})\,\widetilde{\boldsymbol{e}}_y(\alpha_L, z)\right).\end{aligned} \tag{22}$$

Let us introduce $(L+1)\,(2\,N+1)\times 1$ column matrices to express the discretized Fourier coefficients; for example, the Fourier coefficients of $\widetilde{E}_y(x;\alpha_l,z)$ for $l = 0,\ldots,L$ are expressed by a column matrix $\overline{\boldsymbol{e}}_y(z)$ that is defined by

$$\overline{\boldsymbol{e}}_y(z) = \begin{pmatrix}\widetilde{\boldsymbol{e}}_y(\alpha_0, z)\\ \vdots \\ \widetilde{\boldsymbol{e}}_y(\alpha_L, z)\end{pmatrix}, \tag{23}$$

and then Eqs. (15)–(17), and (22) are rewritten as follows:

$$\frac{d}{dz}\,\overline{\boldsymbol{h}}_x(z) - i\,k_0\,\overline{\boldsymbol{X}}\,\overline{\boldsymbol{h}}_z(z) = -i\,k_0\,\overline{\boldsymbol{d}}_y(z) \tag{24}$$

$$\frac{d}{dz}\,\overline{\boldsymbol{e}}_y(z) = -i\,k_0\,\overline{\boldsymbol{h}}_x(z) \tag{25}$$

$$\overline{\boldsymbol{X}}\,\overline{\boldsymbol{e}}_y(z) = \overline{\boldsymbol{h}}_z(z) \tag{26}$$

$$\overline{\boldsymbol{d}}_y(z) = [\![\varepsilon^{(\nu)}]\!]\,\overline{\boldsymbol{e}}_y(z) \tag{27}$$

with

$$\overline{\boldsymbol{X}} = \begin{pmatrix} \boldsymbol{X}(\alpha_0) & \mathbf{0} & \cdots & \mathbf{0} \\ \mathbf{0} & \ddots & \ddots & \vdots \\ \vdots & \ddots & \ddots & \mathbf{0} \\ \mathbf{0} & \cdots & \mathbf{0} & \boldsymbol{X}(\alpha_L) \end{pmatrix} \tag{28}$$

$$[\![\varepsilon^{(\nu)}]\!] = \varepsilon_s\,\boldsymbol{I} + [\![\varepsilon_c^{(\nu)}]\!] \tag{29}$$

$$[\![\varepsilon_c^{(\nu)}]\!] = \frac{1}{2L}\begin{pmatrix} [\![\widetilde{\varepsilon}_c^{(\nu)}]\!](\alpha_0) & 2[\![\widetilde{\varepsilon}_c^{(\nu)}]\!](\alpha_{-1}) & \cdots & 2[\![\widetilde{\varepsilon}_c^{(\nu)}]\!](\alpha_{-L+1}) & [\![\widetilde{\varepsilon}_c^{(\nu)}]\!](\alpha_{-L}) \\ \vdots & \vdots & \ddots & \vdots & \vdots \\ [\![\widetilde{\varepsilon}_c^{(\nu)}]\!](\alpha_L) & 2[\![\widetilde{\varepsilon}_c^{(\nu)}]\!](\alpha_{L-1}) & \cdots & 2[\![\widetilde{\varepsilon}_c^{(\nu)}]\!](\alpha_1) & [\![\widetilde{\varepsilon}_c^{(\nu)}]\!](\alpha_0) \end{pmatrix}. \tag{30}$$

From Eqs. (24)–(27), we obtain the following coupled second-order differential-equation set:

$$\frac{d^2}{dz^2}\,\overline{\boldsymbol{e}}_y(z) = -{k_0}^2\,\boldsymbol{C}_e^{(\nu)}\,\overline{\boldsymbol{e}}_y(z) \tag{31}$$

with

$$\boldsymbol{C}_e^{(\nu)} = [\![\varepsilon^{(\nu)}]\!] - \overline{\boldsymbol{X}}^2. \tag{32}$$

On the other hand, normalized Maxwell's equations and the constitutive relations require that the TM polarized waves satisfy the following relations:

$$\frac{\partial}{\partial z}\,E_x(x,z) - \frac{\partial}{\partial x}\,E_z(x,z) = i\,k_0\,H_y(x,z) \tag{33}$$

$$\frac{\partial}{\partial z}\,H_y(x,z) = i\,k_0\,D_x(x,z) \tag{34}$$

$$\frac{\partial}{\partial x}\,H_y(x,z) = -i\,k_0\,D_z(x,z) \tag{35}$$

$$D_x(x,z) = \varepsilon^{(\nu)}(x)\,E_x(x,z) \tag{36}$$

$$D_z(x,z) = \varepsilon^{(\nu)}(x)\,E_z(x,z) \tag{37}$$

Following the same manipulations with the TE case, we obtain the following relations:

$$\frac{d}{dz}\,\overline{\boldsymbol{e}}_x(z) - i\,k_0\overline{\boldsymbol{X}}\,\overline{\boldsymbol{e}}_z(z) = i\,k_0\,\overline{\boldsymbol{h}}_y(z) \tag{38}$$

$$\frac{d}{dz}\,\overline{\boldsymbol{h}}_y(z) = i\,k_0\,\overline{\boldsymbol{d}}_x(z) \tag{39}$$

$$\overline{\boldsymbol{X}}\,\overline{\boldsymbol{h}}_y(z) = -\overline{\boldsymbol{d}}_z(z) \tag{40}$$

$$\overline{\boldsymbol{d}}_x(z) = [\![\eta^{(\nu)}]\!]^{-1}\,\overline{\boldsymbol{e}}_x(z) \tag{41}$$

$$\overline{\boldsymbol{d}}_z(z) = [\![\varepsilon^{(\nu)}]\!]\,\overline{\boldsymbol{e}}_z(z) \tag{42}$$

where the expression of $[\![\eta^{(\nu)}]\!]$ is given from Eqs. (20), (21), (29), and (30) by replacing the notation ε by η. The inverse expression in Eq. (41) is derived by following Li's Fourier factorization rules [12], and $[\![\eta^{(\nu)}]\!]^{-1}$ can be replaced by $[\![\varepsilon^{(\nu)}]\!]$ only when $\varepsilon^{(\nu)}(x)$ is continuous function. From (38)–(42), we obtain a coupled differential-equation set:

$$\frac{d^2}{dz^2}\,\overline{\boldsymbol{h}}_y(z) = -{k_0}^2\,\boldsymbol{C}_h^{(\nu)}\,\overline{\boldsymbol{h}}_y(z) \tag{43}$$

with

$$\boldsymbol{C}_h^{(\nu)} = [\![\eta^{(\nu)}]\!]^{-1}\left(\boldsymbol{I} - \overline{\boldsymbol{X}}\,[\![\varepsilon^{(\nu)}]\!]^{-1}\,\overline{\boldsymbol{X}}\right). \tag{44}$$

The coupled differential equation sets (31) and (43) can be solved as eigenvalue-eigenvector problems because the matrices of coefficients $\boldsymbol{C}_e^{(\nu)}$ and $\boldsymbol{C}_h^{(\nu)}$ are constant. Let $\boldsymbol{p}_{f,n}^{(\nu)}$ ($f = e, h$ and $n = 1, \ldots, (L+1)\,(2\,N+1)$) be linearly independent eigenvectors of $\boldsymbol{C}_f^{(\nu)}$ corresponding, respectively, to eigenvalues ${\beta_{f,n}^{(\nu)}}^2$. Then the general solution of Eqs. (31) and (43) are written in the following forms:

$$\overline{\boldsymbol{e}}_y(z) = \boldsymbol{P}_e^{(\nu)}\left(\boldsymbol{a}_{e,+}^{(\nu)}(z) + \boldsymbol{a}_{e,-}^{(\nu)}(z)\right) \tag{45}$$

$$\overline{\boldsymbol{h}}_y(z) = \boldsymbol{P}_h^{(\nu)}\left(\boldsymbol{a}_{h,+}^{(\nu)}(z) + \boldsymbol{a}_{h,-}^{(\nu)}(z)\right) \tag{46}$$

with

$$\boldsymbol{P}_f^{(\nu)} = \left(\boldsymbol{p}_{f,1}^{(\nu)} \quad \boldsymbol{p}_{f,2}^{(\nu)} \quad \cdots\right). \tag{47}$$

The column matrices $\boldsymbol{a}_{f,+}^{(\nu)}(z)$ and $\boldsymbol{a}_{f,-}^{(\nu)}(z)$ give the amplitudes of the eigenmodes propagating in the positive and the negative z-directions, respectively, and $\beta_{f,n}^{(\nu)}$ ($n = 1, \ldots, (L+1)\,(2\,N+1)$) give the propagation constants normalized by k_0. Then the z-dependence of $\boldsymbol{a}_{f,\pm}^{(\nu)}(z)$ is expressed by

$$\boldsymbol{a}_{f,\pm}^{(\nu)}(z) = \boldsymbol{U}_f^{(\nu)}(\pm z)\,\boldsymbol{a}_{f,\pm}^{(\nu)}(0) \tag{48}$$

$$\left(\boldsymbol{U}_f^{(\nu)}(z)\right)_{n,m} = \delta_{n,m}\,e^{i\,k_0\,\beta_{f,n}^{(\nu)}\,z}. \tag{49}$$

From Eqs. (25), (39), and (41), we may derive the expressions of $\overline{\boldsymbol{h}}_x(z)$ and $\overline{\boldsymbol{e}}_x(z)$, and we obtain the following relations:

$$\begin{pmatrix} \overline{\boldsymbol{e}}_y(z) \\ \overline{\boldsymbol{h}}_x(z) \end{pmatrix} = \begin{pmatrix} \boldsymbol{P}_e^{(\nu)} & \boldsymbol{P}_e^{(\nu)} \\ \boldsymbol{Q}_e^{(\nu)} & -\boldsymbol{Q}_e^{(\nu)} \end{pmatrix} \begin{pmatrix} \boldsymbol{a}_{e,+}^{(\nu)}(z) \\ \boldsymbol{a}_{e,-}^{(\nu)}(z) \end{pmatrix} \tag{50}$$

$$\begin{pmatrix} \overline{\boldsymbol{h}}_y(z) \\ \overline{\boldsymbol{e}}_x(z) \end{pmatrix} = \begin{pmatrix} \boldsymbol{P}_h^{(\nu)} & \boldsymbol{P}_h^{(\nu)} \\ \boldsymbol{Q}_h^{(\nu)} & -\boldsymbol{Q}_h^{(\nu)} \end{pmatrix} \begin{pmatrix} \boldsymbol{a}_{h,+}^{(\nu)}(z) \\ \boldsymbol{a}_{h,-}^{(\nu)}(z) \end{pmatrix} \tag{51}$$

with

$$\boldsymbol{Q}_e^{(\nu)} = -\boldsymbol{P}_e^{(\nu)}\, \boldsymbol{B}_e^{(\nu)} \tag{52}$$

$$\boldsymbol{Q}_h^{(\nu)} = [\![\eta^{(\nu)}]\!]\, \boldsymbol{P}_h^{(\nu)}\, \boldsymbol{B}_h^{(\nu)} \tag{53}$$

$$\left(\boldsymbol{B}_f^{(\nu)}\right)_{n,m} = \delta_{n,m}\, \beta_{f,n}^{(\nu)}. \tag{54}$$

Equations (50) and (51) give the expression of the modal expansions.

2.3. Scattering Matrix of Cascaded Waveguide Sections

When the fields are computed over the entire structure of cascaded waveguide sections, numerical experiments may show, in many cases, numerical instabilities because of the accumulation of contamination linked with growing exponential functions. To avoid this difficulty, the scattering-matrix (S-matrix) propagation algorithm [13] is applied to derive the relations between the amplitudes of the incoming waves and those of the outgoing waves. Here, we define the S-matrices of the waveguide structure within $z_0 < z < z_\nu$ as follows:

$$\begin{aligned} \begin{pmatrix} \boldsymbol{a}_{f,-}^{(0)}(z_0) \\ \boldsymbol{a}_{f,+}^{(\nu+1)}(z_\nu) \end{pmatrix} &= \boldsymbol{S}_{f,\nu} \begin{pmatrix} \boldsymbol{a}_{f,+}^{(0)}(z_0) \\ \boldsymbol{a}_{f,-}^{(\nu+1)}(z_\nu) \end{pmatrix} \\ &= \begin{pmatrix} \boldsymbol{S}_{f,\nu,11} & \boldsymbol{S}_{f,\nu,12} \\ \boldsymbol{S}_{f,\nu,21} & \boldsymbol{S}_{f,\nu,22} \end{pmatrix} \begin{pmatrix} \boldsymbol{a}_{f,+}^{(0)}(z_0) \\ \boldsymbol{a}_{f,-}^{(\nu+1)}(z_\nu) \end{pmatrix} \end{aligned} \tag{55}$$

for $f = e, h$. The column matrices $\boldsymbol{a}_{f,\pm}^{(0)}(z_0)$ and $\boldsymbol{a}_{f,\pm}^{(\nu+1)}(z_\nu)$ give the modal amplitudes in the 0th-section and $(\nu+1)$th-section, respectively, and the submatrices $\boldsymbol{S}_{f,\nu,pq}$ $(p, q = 1, 2)$ are square matrices in same order. From Eqs. (50) and (51) for $z = z_0$, the initial S-matrix $\boldsymbol{S}_{f,0}$ are derived by follows:

$$\boldsymbol{S}_{f,0,11} = -\boldsymbol{G}_{f,+}^{(1,0)^{-1}}\, \boldsymbol{G}_{f,-}^{(1,0)} \tag{56}$$

$$\boldsymbol{S}_{f,0,12} = \boldsymbol{G}_{f,+}^{(1,0)^{-1}}\, \boldsymbol{Q}_f^{(1)} \tag{57}$$

$$\boldsymbol{S}_{f,0,21} = \boldsymbol{Q}_f^{(1)^{-1}} \left(\boldsymbol{G}_{f,+}^{(1,0)} + \boldsymbol{G}_{f,-}^{(1,0)} \boldsymbol{S}_{f,0,11} \right) \tag{58}$$

$$\boldsymbol{S}_{f,0,22} = \boldsymbol{Q}_f^{(1)^{-1}} \boldsymbol{G}_{f,-}^{(1,0)} \boldsymbol{S}_{f,0,12} \tag{59}$$

where, for $\nu = 0, \ldots, M$, the matrix $\boldsymbol{G}_{f,\pm}^{(\nu+1,\nu)}$ is defined as

$$\boldsymbol{G}_{f,\pm}^{(\nu+1,\nu)} = \frac{1}{2} \left(\boldsymbol{Q}_f^{(\nu+1)} \boldsymbol{P}_f^{(\nu+1)^{-1}} \boldsymbol{P}_f^{(\nu)} \pm \boldsymbol{Q}_f^{(\nu)} \right). \tag{60}$$

Assuming that $\boldsymbol{S}_{f,\nu-1}$ is known for $\nu \geq 1$, Eqs. (48), (50), and (51) yield the expression of $\boldsymbol{S}_{f,\nu}$ as follows:

$$\begin{aligned}
\boldsymbol{S}_{f,\nu} = & \begin{pmatrix} \boldsymbol{0} & \boldsymbol{S}_{f,\nu-1,12} \boldsymbol{U}_f^{(\nu)}(t^{(\nu)}) \\ \boldsymbol{P}_f^{(\nu+1)^{-1}} \boldsymbol{P}_f^{(\nu)} \boldsymbol{U}_f^{(\nu)}(t^{(\nu)}) & \boldsymbol{P}_f^{(\nu+1)^{-1}} \boldsymbol{P}_f^{(\nu)} \end{pmatrix} \\
& \times \begin{pmatrix} \boldsymbol{I} & -\boldsymbol{S}_{f,\nu-1,22} \boldsymbol{U}_f^{(\nu)}(t^{(\nu)}) \\ 2\,\boldsymbol{G}_{f,-}^{(\nu+1,\nu)} \boldsymbol{U}_f^{(\nu)}(t^{(\nu)}) & 2\,\boldsymbol{G}_{f,+}^{(\nu+1,\nu)} \end{pmatrix}^{-1} \\
& \times \begin{pmatrix} \boldsymbol{S}_{f,\nu-1,21} & \boldsymbol{0} \\ \boldsymbol{0} & 2\,\boldsymbol{Q}_f^{(\nu+1)} \end{pmatrix} \\
& + \begin{pmatrix} \boldsymbol{S}_{f,\nu-1,11} & \boldsymbol{0} \\ \boldsymbol{0} & -\boldsymbol{I} \end{pmatrix}
\end{aligned} \tag{61}$$

with $t^{(\nu)} = z_\nu - z_{\nu-1}$. Consequently, the S-matrix $\boldsymbol{S}_{f,M}$ for the entire waveguide structure can be obtained by recursive calculation of Eq. (61) for $\nu = 1, \ldots, M$. Recently, Jia and Yasumoto [14] pointed out that numerical stability is very sensitive to the expressions used on the recursive calculation. The origin of numerical instability has not been clear and the expression for stable calculation is still under consideration. Anyway, we use Eq. (61) as the recursive relation in the following numerical experiments.

3. NUMERICAL EXPERIMENTS

3.1. Propagation Constant

To validate the present formulation, we give below some numerical experiments. In this subsection, we consider a step-index dielectric slab waveguide uniform in the z-direction, and calculate the normalized propagation constants of the fundamental propagation modes, which are obtained as the square roots of the eigenvalues of the matrices $\boldsymbol{C}_e^{(\nu)}$

and $\boldsymbol{C}_h^{(\nu)}$ given in Eqs. (32) and (44). The parameters of the waveguide are chosen as the wavelength $\lambda_0 = 1\,\mu$m, the refractive index of core $n_c = 1.54$, the refractive index of cladding $n_s = 1.52$, and the width of core $a = 0.5\,\lambda_0$. The exact values of the normalized propagation constants can be obtained by solving the dispersion equations, and they are given as $\beta_{\mathrm{TE}} \approx 1.52253929492$ and $\beta_{\mathrm{TM}} \approx 1.52243893928$ for the fundamental modes in the TE and the TM polarizations, respectively. Figure 2 shows the error rate of the propagation constants $|\beta - \beta_{\mathrm{ex}}|\,/\beta_{\mathrm{ex}}$ as functions of the truncation order N that truncates the Fourier series expansions from $-N$th to Nth-order, where β_{ex} denotes the exact propagation constant. The curves show the results obtained by the present formulation with the number of integration segments $L = 30$, which discretized the integration interval $0 \le \alpha \le 2\,\pi/d$ with $L + 1$ equally spaced points. Comparing the numerical results with the fictitious periods $d = \lambda_0$, $2\,\lambda_0$, and $5\,\lambda_0$, the calculated propagation constants converge smoothly, and small period shows rapid convergence. However, the numerical results do not converge for the smaller fictitious periods $d = 0.2\,\lambda_0$ and $0.5\,\lambda_0$.

Next, we consider the convergence with respect to the number of integration segments L. The numerical results shown in Fig. 3 are computed by the present formulation with the same parameters as for Fig. 2, but we use the truncation order of $N = 15$. The results of larger fictitious period show more rapid convergence but those show also worse accuracy limit. This accuracy limit is determined by the truncation order N, and it becomes smaller if we use larger fictitious period. Conversely, calculation with the small fictitious period requires large number of integration segments to obtain precise results and this is the reason why the results with small fictitious periods do not converge in Fig. 2. The number of integration segments $L = 30$ is not enough to use the small fictitious periods $d = 0.2\,\lambda_0$ or $0.5\,\lambda_0$ and they must show reliable convergences if we use large L. The order of matrices $\boldsymbol{C}_e^{(\nu)}$ and $\boldsymbol{C}_h^{(\nu)}$ is $(L+1)\,(2\,N+1)$ and that in FSEM is $2\,N+1$. FSEM does not use the α-dependence and all matrices are calculated at $\alpha = 0$. Then FSEM requires large fictitious period to obtain a rapid convergence with respect to L and, as the result, the convergence with respect to N becomes slow. Consequently, the matrix order of the present formulation becomes comparable with that of FSEM.

3.2. Off-Axis Connections

This subsection deals with the waveguide structure with two step discontinuities at $z = z_0$ and $z = z_1$ shown in Fig. 4. The parameters of

the waveguide are chosen as same with those in Ref. [9]; the wavelength $\lambda_0 = 0.83\,\mu$m, the refractive index of core $n_c = 3.44$, the refractive index of cladding $n_s = 3.29$, and the width of core $a = 0.48\,\lambda_0$. The waveguide supports only one guided mode. The place of step

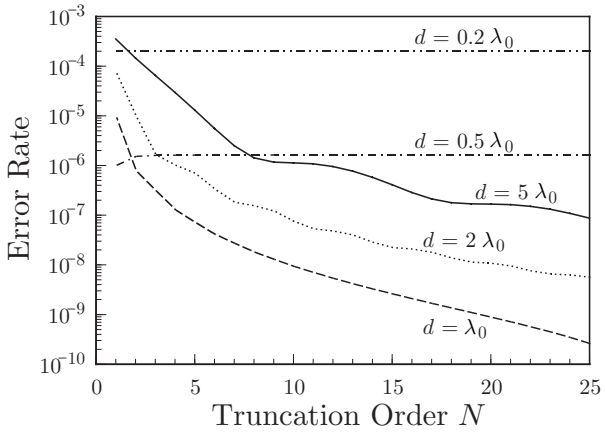

(a) TE polarization

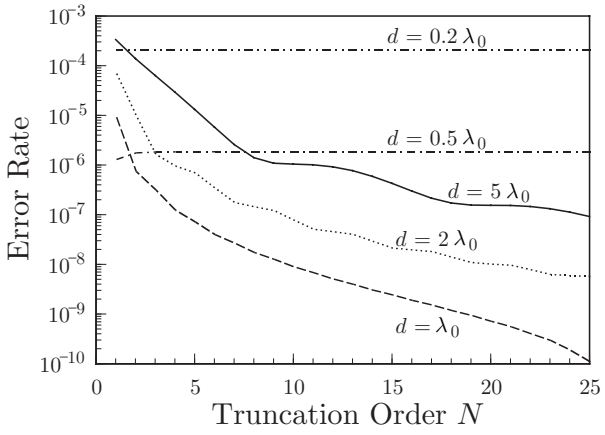

(b) TM polarization

Figure 2. Error rate of the propagation constants of a step-index dielectric slab waveguide as function of the truncation order N with the number of Integration segments $L = 30$. The waveguide parameters are chosen as the core index 1.54, the cladding index 1.52, the core width $0.5\,\mu$m, and the different fictitious period d for free space wavelength of $1\,\mu$m.

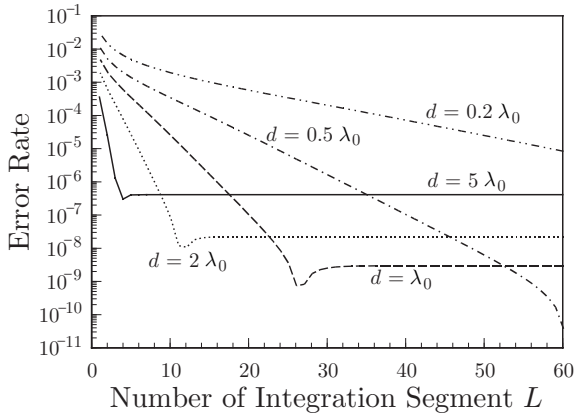

(a) TE polarization

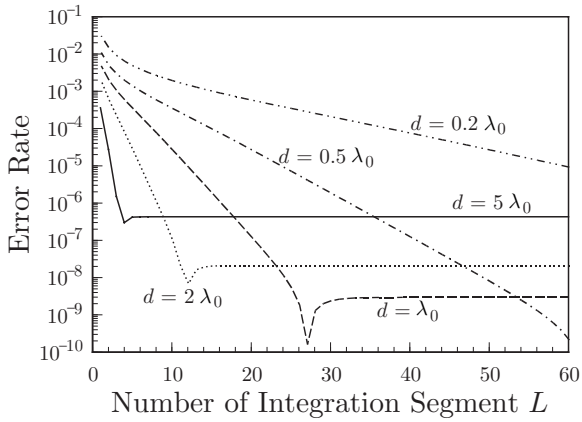

(b) TM polarization

Figure 3. Error rate of the propagation constants as function of the number of Integration segments L with the truncation order $N = 15$. The values of waveguide parameters are the same as those in Fig. 2.

transitions are specified by $z_0 = \lambda_0$ and $z_1 = 41\,\lambda_0$, and the waveguide axis shifts by the core width a in the region $z_0 < z < z_1$. We assume that the rightward propagating fundamental guided mode with a unit power from the waveguide section 0 ($z < z_0$) and the power transmission coefficients can be calculated by using the amplitude of the rightward propagating fundamental guided mode in the waveguide Section 2 ($z > z_1$). In this structure, a strong radiation occurs at the

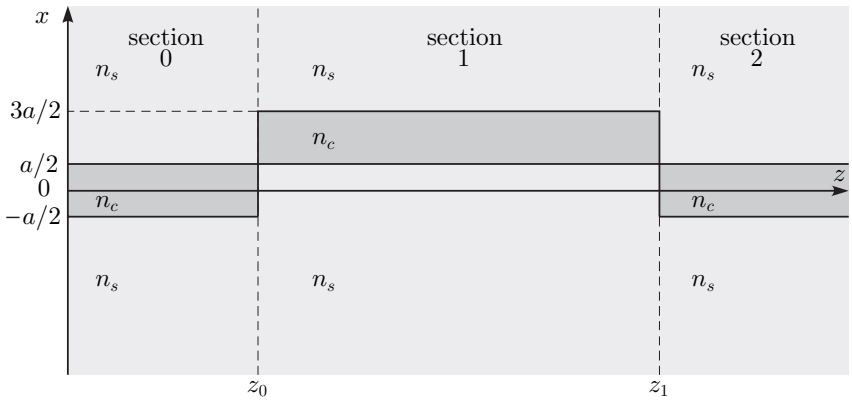

Figure 4. Dielectric slab waveguide with two off-axis connections under consideration.

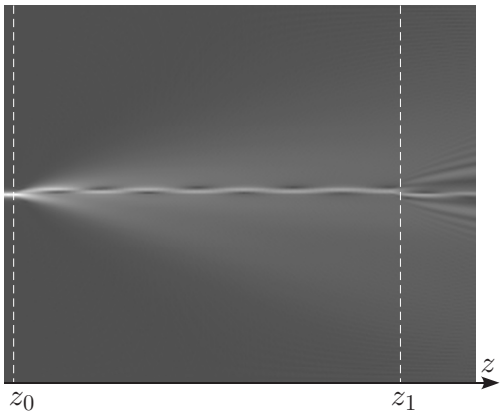

Figure 5. Field distribution along the waveguide shown in Fig. 4 calculated in the TE polarization for $d = 2\,\lambda_0$, $L = 20$, and $N = 15$. The parameters are chosen as $\lambda_0 = 0.83\,\mu$m, $n_c = 3.44$, $n_s = 3.29$, and $a = 0.48\,\lambda_0$.

plane of the first discontinuity located at $z = z_0$, and the radiated wave is coupled at $z = z_1$ with the guided mode of the waveguide Section 2. Therefore an appropriate treatment of the radiated wave is necessary for precise calculation. Figure 5 shows the E_y field distribution (TE polarization) along the waveguide calculated for $d = 2\,\lambda_0$, $L = 20$, and $N = 15$. The distribution seems to be good agreement with that in Fig. 3 of Ref. [9]. Figure 6 shows convergences of the power

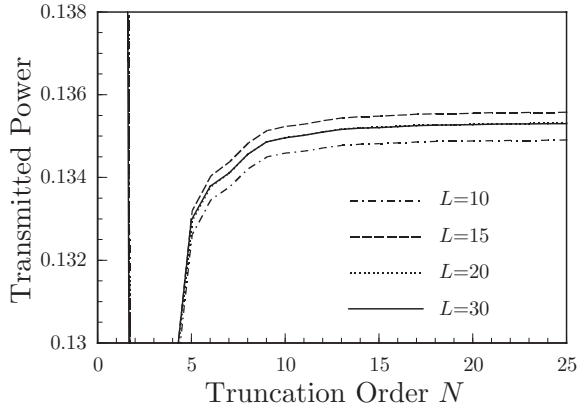

(a) TE polarization

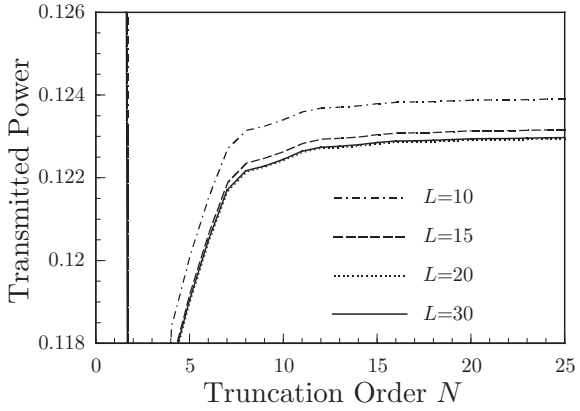

(b) TM polarization

Figure 6. Convergence of the power transmission coefficients for the guided modes in the waveguide structure with two off-axis connections shown in Fig. 4. The values of waveguide parameters are the same as those in Fig. 5, and the coefficients are calculated for $d = 2\,\lambda_0$ and the different numbers of integration segments L.

transmission coefficients for the guided modes as functions of the truncation order N. The curves are the results obtained with the fixed fictitious period $d = 2\,\lambda_0$ and the several numbers of integration segments L. The results provide reliable convergences, and the values for $L = 30$ and $N = 25$ are 0.13530 in TE polarization and 0.12297 in TM polarization. Unfortunately, it is impossible to know the exact values of the power transmission coefficients for this problem.

However, FSEM with the fictitious period $d = 40\,\lambda_0$ and the truncation order $N = 300$ gives 0.1352 in TE polarization and 0.1228 in TM polarization, which are in good agreement with the results of the present formulation.

4. CONCLUSIONS

A novel formulation for series of waveguide transitions has proposed based on the periodic Fourier transform that makes functions periodic and then the transformed functions can be approximately expanded in the truncated Fourier series. The Fourier coefficients are functions of the transform parameter, which is denoted by α in this paper, and the coefficients have been discretized with respect to the transform parameter. Then, wave propagation in the waveguide structure is described by matrix relations and the problem can be solved as an eigenvalue-eigenvector problem. The present formulation has applied to a straight dielectric slab waveguide and obtained propagation constants converged to the exact values. The formulation was also applied to a waveguide structure with two step discontinuities and the obtained values of the power transmission coefficients were in good agreement with the results of FSEM. This paper considered only two-dimensional structures of waveguide transitions. However, there is no doubt that extensions to three-dimensional problems could be also done at the cost of some additional work.

APPENDIX A. CONVERGENCE OF PERIODIC FOURIER TRANSFORM

Let $\{\widetilde{f}_N(x;\alpha)\}$ $(N = 1, 2.3, \dots)$ be a functional sequence defined by

$$\widetilde{f}_N(x;\alpha) = \sum_{m=-N}^{N} f(x - m\,d)\, e^{i\,\alpha(x-m\,d)}. \tag{A1}$$

In Eq. (A1), we assume that the function f satisfies the following conditions (f1)–(f3):

(f1) f is absolutely integrable in $(-\infty, \infty)$; that is, $\int_{-\infty}^{\infty} |f(x)|\,dx < \infty$.

(f2) $|f|$ is uniformly bounded in $(-\infty, \infty)$.

(f3) There exists a positive number K such that $|f(x)|$ is non-decreasing for $x \in (-\infty, -K)$, and $|f(x)|$ is non-increasing for $x \in (K, \infty)$.

Theorem 1. *If the conditions* (f1)–(f3) *hold, then* $\{\widetilde{f}_N(x;\alpha)\}$ *pointwisely converges to a certain function* $\widetilde{f}(x;\alpha) = \sum_{m=-\infty}^{\infty} f(x - m\,d)\,e^{-i\,\alpha(x-m\,d)}$ *as* $N \to \infty$. *That is,*

$$\lim_{N\to\infty} \left|\widetilde{f}(x;\alpha) - \widetilde{f}_N(x;\alpha)\right| = 0 \tag{A2}$$

for each fixed $x \in (-\infty, \infty)$.

Proof. Let M and N be natural numbers with $M < N$. For any fixed $x \in (-\infty, \infty)$, it follows from Eq. (A1) that

$$\begin{aligned}
&\left|\widetilde{f}_N(x;\alpha) - \widetilde{f}_M(x;\alpha)\right| \\
&= \left|\sum_{m=-N}^{N} f(x - m\,d)\,e^{-i\,\alpha(x-m\,d)} - \sum_{m=-M}^{M} f(x - m\,d)\,e^{-i\,\alpha(x-m\,d)}\right| \\
&= \left|\left(\sum_{m=-N}^{-M-1} + \sum_{m=M+1}^{N}\right) f(x - m\,d)\,e^{-i\,\alpha(x-m\,d)}\right| \\
&\le \left(\sum_{m=-N}^{-M-1} + \sum_{m=M+1}^{N}\right) |f(x - m\,d)| \\
&= \frac{1}{d}\left(\sum_{m=M+1}^{N} |f(x - m\,d)|\,d + \sum_{m=M+1}^{N} |f(x + m\,d)|\,d\right).
\end{aligned} \tag{A3}$$

Since x is fixed, we can choose a large integer M such that

$$|x \pm m\,d| > K \quad \text{for} \quad m = M, M+1, M+2, \ldots, N. \tag{A4}$$

Here K is the positive number introduced by (f3). By the monotone condition (f3) and Eq. (A4), we can observe

$$\begin{cases} |f(x - m\,d)| \le |f(y)| & \text{if } y \in [x - m\,d, x - (m-1)\,d] \\ |f(x + m\,d)| \le |f(y)| & \text{if } y \in [x + (m-1)\,d, x + m\,d] \end{cases} \tag{A5}$$

for all $m = M+1, M+2, \ldots, N$. Therefore, if M and N are large

enough, then Eqs. (A3) and (A5) yield

$$\begin{aligned}\sum_{m=M+1}^{N} |f(x-m\,d)|\,d + \sum_{m=M+1}^{N} |f(x+m\,d)|\,d \\ \leq \left(\int_{x-Nd}^{x-Md} + \int_{x+Md}^{x+Nd}\right) |f(y)|\,dy \\ \leq \left(\int_{-\infty}^{x-Md} + \int_{x+Md}^{\infty}\right) |f(y)|\,dy. \qquad \text{(A6)}\end{aligned}$$

Hence it turns out from Eqs. (A3) and (A6) that

$$\left|\widetilde{f}_N(x;\alpha) - \widetilde{f}_M(x;\alpha)\right| \leq \frac{1}{d}\left(\int_{-\infty}^{x-Md} + \int_{x+Md}^{\infty}\right) |f(y)|\,dy. \qquad \text{(A7)}$$

Since f is absolutely integrable in $(-\infty,\infty)$ (see (f1)), we know

$$\lim_{M\to\infty}\left(\int_{\infty}^{K-Md} + \int_{x+Md}^{\infty}\right) |f(y)|\,dy = 0. \qquad \text{(A8)}$$

By taking account for $M < N$, we obtain from Eqs. (A7) and (A8)

$$\lim_{M,N\to\infty}\left|\widetilde{f}_N(x;\alpha) - \widetilde{f}_M(x;\alpha)\right| = 0, \qquad \text{(A9)}$$

which means that $\{\widetilde{f}_N(x,\alpha)\}$ gives a Cauchy sequence in $\boldsymbol{R}$. Therefore, we have proved the convergence (A2). □

Remark 2. *The monotone property* (f3) *is not a technical condition for the convergence of* $\{\widetilde{f}_N(x;\alpha)\}$. *Indeed, under the assumption that* $f(x)$ *is piecewise continuous and absolutely integrable in* $(-\infty,\infty)$, *there exists a counterexample which diverges.*

For all integers $m(=\pm1,\pm2,\dots)$ except 0, we define a function $f(x)$ by

$$f(x) = \begin{cases} 1 & \text{if } x \in \left[2\,m\,\pi - \dfrac{1}{2\,m^2},\ 2\,m\,\pi + \dfrac{1}{2\,m^2}\right], \\ 0 & \text{otherwise.}\end{cases} \qquad \text{(A10)}$$

Then $f(x)$ is a piecewise continuous function which possesses infinitely many discontinuous points. Furthermore, we observe that

$$\int_{-\infty}^{\infty} |f(x)|\,dx = 2\left(\sum_{m=1}^{\infty}\frac{1}{m^2}\right) = \frac{\pi^2}{3}. \qquad \text{(A11)}$$

Hence Eq. (A11) implies that f is absolutely integrable in $(-\infty, \infty)$. Since

$$f(-2\,m\,\pi) = 1 \quad \text{for all} \quad m = \pm 1, \pm 2, \dots , \tag{A12}$$

then letting $(x, d, \alpha) = (0, 2\,\pi, 1)$ in Eq. (A1) enables us to know

$$\begin{aligned} \widetilde{f}_N(0;1) &= \sum_{m=-N,\, m\neq 0}^{N} f(0 - m\,d)\, e^{-i\,m\,d} \\ &= \sum_{m=-N,\, m\neq 0}^{N} f(-2\,m\,\pi)\, e^{-i\,2\,m\,\pi} \\ &= \sum_{m=-N,\, m\neq 0}^{N} e^{-i\,2\,m\,\pi} \\ &= \sum_{m=-N,\, m\neq 0}^{N} 1 \\ &= 2N. \end{aligned} \tag{A13}$$

Consequently, Eq. (A13) leads to

$$\lim_{N\to\infty} \widetilde{f}_N(0;1) = \lim_{N\to\infty} 2N = \infty. \tag{A14}$$

Thus the above $\{\widetilde{f}_N(x;1)\}$ gives a desired counterexample.

Remark 3. *Even in the case when f is smooth and absolutely integrable in $(-\infty, \infty)$, the sequence $\{\widetilde{f}_N(x;1)\}$ in Eq. (A1) does not necessarily converge.*

For $m(= \pm 1, \pm 2, \dots)$, let $\rho_m(x)$ be a smooth nonnegative function such that

$$\operatorname{supp} \rho_m = \left\{ -\frac{1}{2\,m^2} \le x \le \frac{1}{2\,m^2} \right\} \quad \text{and} \quad \int_{-\infty}^{\infty} \rho_m(x)\, dx = 1. \tag{A15}$$

Here $\operatorname{supp} \rho_m$ represents the closure of the interval with $\rho_m(x) > 0$. For the function f defined in Eq. (A10), we can construct a smooth perturbation of f by

$$f^*(x) = \begin{cases} \displaystyle\int_{-\infty}^{\infty} \rho_m(x-y) f(y)\, dy & \text{if } x \in \left[2m\pi - \frac{1}{m^2}, 2m\pi + \frac{1}{m^2} \right], \\ 0 & \text{otherwise.} \end{cases} \tag{A16}$$

It should be noted that the above smoothing construction technique is well known in the field of differential equations (see e.g., Evans [15, APPENDIX C]). It is possible to prove that f^* is a smooth nonnegative function in $(-\infty, \infty)$. Further, from Eq. (A15) we can easily verify that

$$\begin{aligned}\int_{-\infty}^{\infty} |f^*(x)|\, dx &= \int_{-\infty}^{\infty}\int_{-\infty}^{\infty} \rho_m(x-y)\, f(y)\, dx\, dy \\ &= \int_{-\infty}^{\infty} f(x)\, dx. \end{aligned} \tag{A17}$$

In view of Eq. (A11), we know that f^* is absolutely integrable in $(-\infty, \infty)$. It follows from Eqs. (A10) and (A15) that

$$\begin{aligned} f^*(2\,m\,\pi) &= \int_{-\infty}^{\infty} \rho_m(2\,m\,\pi - y)\, f(y)\, dy \\ &= \int_{-\frac{1}{2\,m^2}}^{\frac{1}{2\,m^2}} \rho_m(y)\, f(2\,m\,\pi - y)\, dy \\ &= \int_{-\frac{1}{2\,m^2}}^{\frac{1}{2\,m^2}} \rho_m(y)\, dy \\ &= 1 \end{aligned} \tag{A18}$$

for all $m(= \pm 1, \pm 2, \dots)$. Since $f^*(-2\,m\,\pi) = 1$ for such m, the same procedure as Eq. (A13) leads to $\lim_{N\to\infty} \widetilde{f}_N(0;1) = \lim_{N\to\infty} 2N = \infty$, when $(x, d, \alpha) = (0, 2\,\pi, 1)$ in Eq. (A1).

REFERENCES

1. Marcuse, D., *Theory of Dielectric Optical Waveguides*, Academic Press, New York, 1974.
2. Burns, W. K., "Normal mode analysis of waveguide devices," *IEEE J. Lightwave Technol.*, Vol. LT-6, No. 6, 1051–1068, 1988.
3. Feit, M. D. and J. A. Fleck, Jr., "Calculation of dispersion in graded-index multimode fibers by a propagation-beam method," *Appl. Opt.*, Vol. 18, No. 16, 2843–2851, 1979.
4. Chung, Y. and N. Dagli, "An assessment of finite difference beam propagation method," *IEEE J. Quantum Electron.*, Vol. 26, No. 8, 1335–1339, 1990.
5. Henry, C. H. and Y. Shani, "Analysis of mode propagation in optical waveguide devices by Fourier expansion," *IEEE J. Quantum Electron.*, Vol. QE-27, No. 3, 523–530, 1991.

6. Hosono, T., T. Hinata, and A. Inoue, "Numerical analysis of the discontinuities in slab dielectric waveguides," *Radio Sci.*, Vol. 17, 75–83, 1982.
7. Yamakita, Y., K. Matsumoto, and K. Rokushima, "Analysis of discontinuities in anisotropic dielectric waveguides," IEICE Tech. Rep., EMT-93-87, 81–90, 1993.
8. Silberstein, E., P. Lalanne, J. P. Hugonin, and Q. Cao, "Use of grating theories in integrated optics," *J. Opt. Soc. Am. A*, Vol. 18, 2865–2875, 2001.
9. Yasumoto, K., K. Watanabe, and J. Ishihara, "Numerical analysis of optical waveguides with the use of Fourier-series expansion method combined with perfectly matched layer," *Microwave and Opt. Technol. Lett.*, Vol. 34, No. 6, 422–426, 2002.
10. Nakayama, J., "Periodic Fourier transform and its application to wave scattering from a finite periodic surface," *IEICE Trans. Electron.*, Vol. E83-C, No. 3, 481–487, 2000.
11. Nakayama, J., "Periodic Fourier transform and its application to wave scattering from a finite periodic surface: Two-dimensional case," *IEICE Trans. Electron.*, Vol. E88-C, No. 5, 1025–1032, 2005.
12. Li, L., "Use of Fourier series in the analysis of discontinuous periodic structures," *J. Opt. Soc. Am. A*, Vol. 13, No. 9, 1870–1876, 1996.
13. Li, L., "Formulation and comparison of two recursive matrix algorithms for modeling layered diffraction gratings," *J. Opt. Soc. Am. A*, Vol. 13, No. 5, 1024–1035, 1996.
14. Jia, H. and K. Yasumoto, "A novel formulation of the Fourier model method in S-matrix form for arbitrary shaped gratings," *Int. J. Infrared and Millimeter Waves*, Vol. 25, No. 11, 1591–1609, 2004.
15. Evans, L. C., "Partial differential equations," *Graduate Studies in Mathematics*, Vol. 19, Am. Math. Soc., Providence, RI, 1998.